How to cite: *Angew. Chem. Int. Ed.* **2024**, *63*, e202315887
doi.org/10.1002/anie.202315887

Polymer Chemistry | Hot Paper

Main-chain Macromolecular Hydrazone Photoswitches

Linh Duy Thai[+], *Julian Fanelli*[+], *Rangika Munaweera, Megan L. O'Mara,* Christopher Barner-Kowollik,* and Hatice Mutlu**

Abstract: Hydrazones—consisting of a dynamic imine bond and an acidic NH proton—have recently emerged as versatile photoswitches underpinned by their ability to form thermally bistable isomers, (*Z*) and (*E*), respectively. Herein, we introduce two photoresponsive homopolymers containing structurally different hydrazones as main-chain repeating units, synthesized via head-to-tail Acyclic Diene METathesis (ADMET) polymerization. Their key difference lies in the hydrazone design, specifically the location of the aliphatic arm connecting the rotor of the hydrazone photoswitch to the aliphatic polymer backbone. Critically, we demonstrate that their main photoresponsive property, i.e., their hydrodynamic volume, changes in opposite directions upon photoisomerization ($\lambda = 410$ nm) in dilute solution. Further, the polymers—independent of the design of the individual hydrazone monomer—feature a photoswitchable glass transition temperature (T_g) by close to 10 °C. The herein established design strategy allows to photochemically manipulate macromolecular properties by simple structural changes.

Introduction

Light is a powerful trigger for chemical transformations due to its traceless nature as well as the spatiotemporal control it offers.[1] Photoresponsive chemical compounds which reversibly change their configuration via isomerization and/or cyclization, such as azobenzenes,[2] stilbenes,[3] spiropyrans[4]/spirooxazines,[5] diarylethenes,[6] have frequently been integrated into photoresponsive polymeric materials.[7] Key applications of such polymers range from information encoding/data storage[8] to metal ions probing[5a] as well as photopatterning.[9] Recently, α-bisimines[10] and hydrazones[11] have emerged as promising photoswitches. Interestingly, several hydrazones, which are derivatives of imines, are capable of switching from one thermodynamically stable isomer to another, with a low thermal half-life (≈300–5000 years) at ambient temperatures, making the forward and back isomerization exclusively controlled by light.[11–12] More importantly, the hydrazone photoswitch shows an impressively high stability upon multiple cycles of photoisomerization.[11,13,23]

Synthetically, reversible deactivation radical polymerization (RDRP) techniques, e.g., Atom Transfer Radical Polymerization (ATRP)[14] or Reversible Addition Fragmentation chain-Transfer (RAFT)[15] polymerization have routinely been deployed to construct photoswitchable polymers with the photoactive groups embedded in their side chains. However, it is preferable to place photoswitches into the backbone of the polymer chain as the impact on the resulting polymer properties such as electron conductivity[16] or hydrodynamic volume[10b] is likely to be more significant. The construction of main-chain photoswitchable polymers has been realized by Ring Opening Metathesis Polymer-

[*] Dr. H. Mutlu
Institut de Science des Matériaux de Mulhouse (IS2M), UMR 7361 CNRS/Université de Haute Alsace (UHA)
15 rue Jean Starcky, 68057 Mulhouse Cedex (France)
E-mail: hatice.mutlu@uha.fr

L. D. Thai,[+] J. Fanelli,[+] Prof. C. Barner-Kowollik
School of Chemistry and Physics, Queensland University of Technology (QUT)
2 George Street, 4000 Brisbane, QLD (Australia)
and
Centre for Materials Science, Queensland University of Technology (QUT)
2 George Street, 4000 Brisbane, QLD (Australia)
and
Institute of Nanotechnology (INT), Karlsruhe Institute of Technology (KIT)
Hermann-von-Helmholtz-Platz 1, 76344 Eggenstein-Leopoldshafen (Germany)
E-mail: christopher.barnerkowollik@qut.edu.au
christopher.barner-kowollik@kit.edu

R. Munaweera, Prof. M. L. O'Mara
Australian Institute for Bioengineering and Nanotechnology (AIBN), The University of Queensland (UQ)
4067 St Lucia, QLD (Australia)
E-mail: m.omara@uq.edu.au

J. Fanelli[+]
Soft Matter Synthesis Laboratory, Institute for Biological Interfaces 3, Karlsruhe Institute of Technology (KIT)
Hermann-von-Helmholtz-Platz 1, 76344 Eggenstein-Leopoldshafen (Germany)

[+] These authors contributed equally to this work.

ization (ROMP)[17] and (head-to-tail) Acyclic Diene METathesis (ADMET) polymerization.[10b,c,18] By virtue of head-to-tail ADMET polymerization, the formation of internal acrylate double bonds in the resulting polymers allows for post-polymerization modification. We have recently demonstrated the utilization of thiol-Michael reactions to attach C_{12}-alkyl thiols as side chains to parent α-bisimine-based ADMET homopolymers, leading to a critical enhancement in the solid-state isomerization of α-bisimine photoswitches.[18] While main-chain polymers based on azobenzenes and α-bisimine have been synthesized via ADMET,[10c,18,20] the application of this technique to prepare hydrazone-based main-chain photoswitchable polymers remains unexplored.

Furthermore, for main-chain stimuli-responsive polymeric materials, the connection point where the stimuli-sensitive groups are covalently installed into the polymer backbone impacts the behavior of macromolecules. For example, Craig et al. reported three similar mechano-responsive elastomers derived from three main-chain spiropyran regioisomers.[21] Their results demonstrated different colorimetric responses from the three elastic polymer films upon stretching.[21] Inspired by these regiochemical effects, we herein explore if—for instance—changes in hydrodynamic volume occur if the substitution position of the arm connecting the rotor of the hydrazone photoswitch to the polymer main-chain is switched from one side to another (refer to Design **1** vs Design **2** in Scheme 1).

Over the past years, we have unambiguously demonstrated that absorptivity (represented as an absorption spectrum) is no predictor for photochemical reactivity in solution, demonstrated in a wide array of photochemical action plots.[22] Establishing the wavelength-dependent reactivity of photochemical reactions, including photoisomerization, is thus critical, also in our current exploration of main-chain hydrazone containing polymers.

Herein, we report the synthesis and solution photoisomerization of two photoreactive homopolymers, $\mathbf{P_{h1}}$ and $\mathbf{P_{h2}}$, consisting of repeating hydrazone moieties in their backbone. These light-sensitive polymers were obtained via head-to-tail ADMET polymerization, allowing for the construction of defined polymer architectures. In both designs, i.e., polymer $\mathbf{P_{h1}}$ and $\mathbf{P_{h2}}$, the stator (yellow phenyl ring, according to Scheme 1) is *ortho*-substituted with the imine bond and with one of the two essential reactive handles for the ADMET polymerization (i.e., an acrylate). In design **1**, i.e., $\mathbf{P_{h1}}$, the rotor is decorated with a phenyl ring that is substituted on the *para*-position with the polymerizable handle (i.e., the olefin) and the acetyl functional moiety, which acts as an *H*-bond acceptor. In design **2**, i.e., $\mathbf{P_{h2}}$, the phenyl rotor is non-substituted and the functional group (i.e., the ester group shown in green in Scheme 1), which serves as the *H*-bond acceptor, also provides the polymerizable functional unit (i.e., the olefin handle). The key design differences between the two polymers thus are (*i*) the position of one of the two arms connecting the rotor of the photoswitch to the backbone (Scheme 1, Figure 1A, D) and (*ii*) one additional ester group (–COOR) in the phenyl rotor of $\mathbf{P_{h1}}$ (Scheme 1, Figure 1A, D).

We investigate the isomerization of the photoswitching polymers using a wavelength-tunable laser system. Interestingly, the photoisomerization kinetics of the two polymers, $\mathbf{P_{h1}}$ and $\mathbf{P_{h2}}$, are distinctively different, with $\mathbf{P_{h1}}$ isomerizing close to two times faster. Further, Size-Exclusion Chromatography (SEC) reveals a surprising antagonistic change in

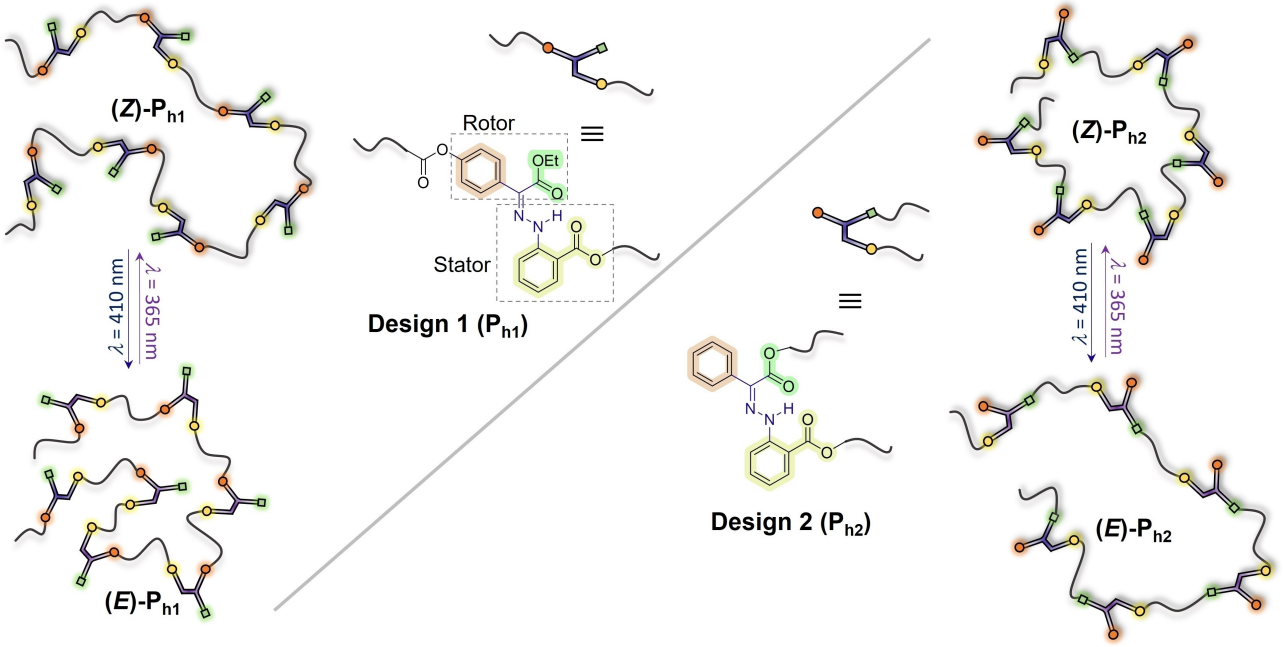

Scheme 1. Design strategy for two main-chain hydrazone polymers, enabling opposite changes in hydrodynamic volume upon photoisomerization of the hydrazone core. The taxonomy of the rotor and stator is adapted from the work of Aprahamian and colleagues.[19]

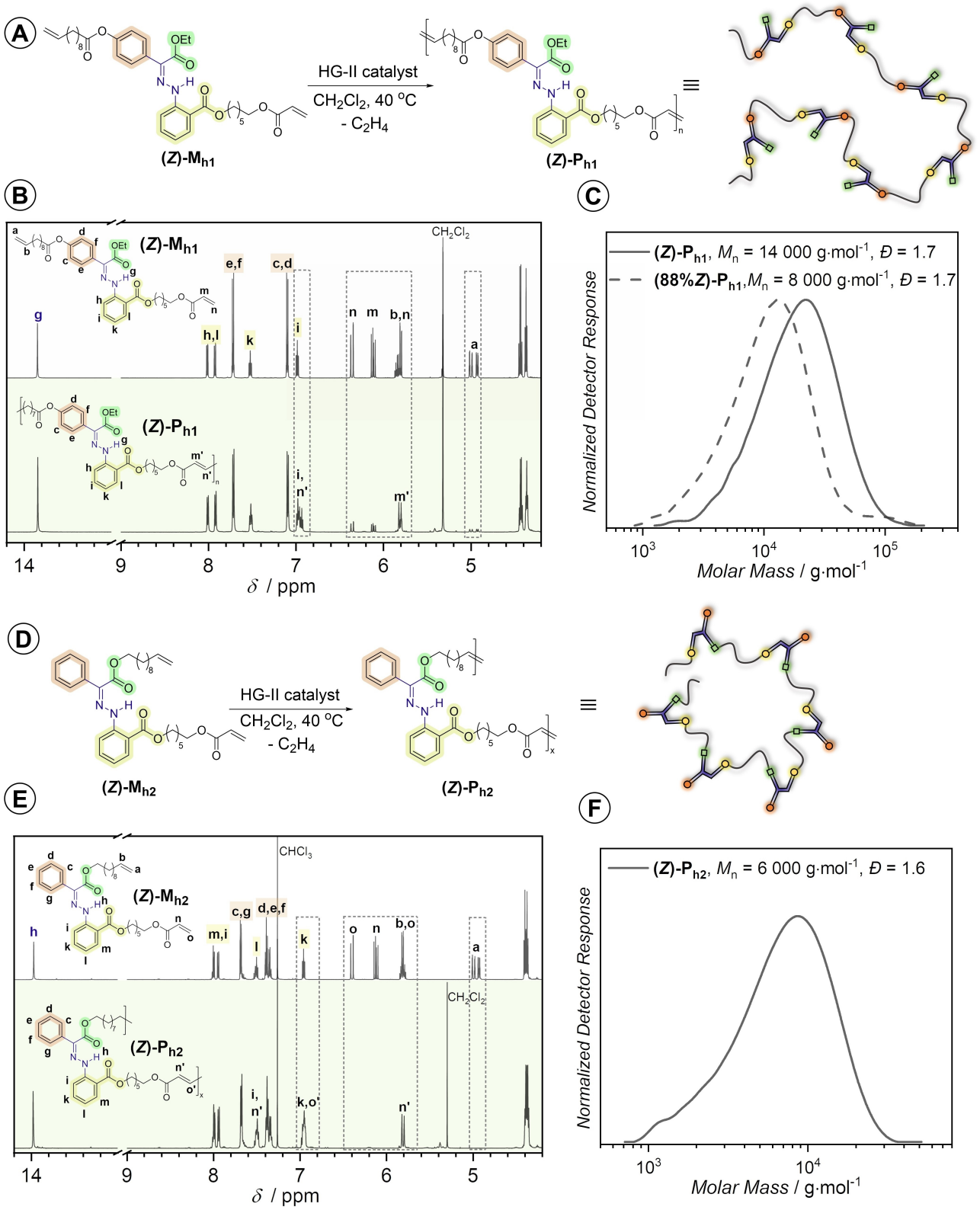

Figure 1. Representation of the hydrazone core unit synthesis (A, D), in addition to their ^{1}H NMR spectra recorded in either CD_2Cl_2 or $CDCl_3$ (B, E), and SEC traces (C, F) of polymer $\mathbf{P_{h1}}$ and $\mathbf{P_{h2}}$ recorded in dimethylacetamide (DMAc), respectively. HG-II: Hoveyda-Grubbs 2nd generation catalyst. M_n represents the apparent number-averaged molar mass.

the molecular weight distribution of the homopolymers (up to 25 % change in peak molecular weight) upon the forward and back photoisomerization at 410 nm and 365 nm, respectively. Further, the installation of the hydrazones in the polymer backbone reduces their glass transition temperature (T_g) by up to approximately 10 °C, for both $\mathbf{P_{h1}}$ and $\mathbf{P_{h2}}$ upon blue light irradiation (400-nm LEDs), which is in contrast to the results obtained from side-chain containing hydrazone polymers reported in the literature.[23]

Results and Discussion

We designed two ADMET monomers featuring a hydrazone core as the main-chain chromophore (Figure 1A, D). While the stators of the photoswitch in the two designs are identical, the substitution position of the arm containing the alkene functional group in the rotors is different for monomer $\mathbf{M_{h1}}$ and $\mathbf{M_{h2}}$. Further, we placed an additional ester functionality in the rotor of $\mathbf{M_{h1}}$ as noted above (Figure 1A, D). Synthetically, the pure (*Z*)-isomer of $\mathbf{M_{h2}}$ (denoted **(*Z*)-$\mathbf{M_{h2}}$**) was obtained without difficulty, whereas significantly more purification effort was needed to acquire the pure (*Z*)-configuration of $\mathbf{M_{h1}}$ (denoted **(*Z*)-$\mathbf{M_{h1}}$**). However, we are also interested in investigating the effect of isomer mixtures in $\mathbf{M_{h1}}$ (88 % (*Z*)- and 12 % (*E*)-isomers), denoted **(88 %Z)-$\mathbf{M_{h1}}$** on the final number-averaged molar mass (M_n) of the resulting polymers.

To fabricate the main-chain photoswitchable polymers, we employed head-to-tail ADMET polymerization using a Hoveyda-Grubbs 2nd generation catalyst (HG-II) and dichloromethane (DCM) as the solvent. DCM is an effective solvent for cross-metathesis reactions, typically affording polymers with relatively high M_n.[24] The gradual disappearance of the magnetic resonances corresponding to the terminal alkene (4.96 and 5.83 ppm) and acrylate groups (5.80, 6.11 and 6.36 ppm) alongside the appearance of the internal acrylate bonds (5.81 and 6.96 ppm) as indicated in Figure 1 confirms the high selectivity of the cross-metathesis polymerization. Despite the capability of hydrazones to form complexes with metal ions,[25] ADMET polymerization of the designed hydrazone monomers proceeded smoothly under the catalysis of Ru-centered HG-II. As evidenced by the ^{1}H NMR spectra depicted in Figure 1, there is no evident shift of the magnetic resonances associated with the hydrazone core, especially the resonances of the aromatic hydrogens, which are sensitive to complexation of the azomethine nitrogen to Ru.

We designed a hydrazone core featuring two ester groups in close proximity to the hydrazone hydrogen (highlighted as green and yellow in Figure 1A, D), which act as strong hydrogen acceptors. This, in turn, hindered access of the Ru-based ADMET catalyst to the photoswitchable core.[26] The apparent number average molecular weights, M_n, of the resulting polymers, **(*Z*)-$\mathbf{P_{h1}}$**, **(88 %Z)-$\mathbf{P_{h1}}$**, and **(*Z*)-$\mathbf{P_{h2}}$**, are close to 14000, 8000, and 6000 g·mol^{-1} on the basis of a poly(methyl methacrylate) (PMMA) calibration, respectively (Figure 1). The M_n of **(*Z*)-$\mathbf{P_{h1}}$** is comparable with the values reported for other main-chain photoresponsive polymers based on α-bisimine and azobenzene units.[18,27] In contrast, with 12 % of (*E*)-isomer in **(88 %Z)-$\mathbf{M_{h1}}$**, the M_n of the resulting polymer (**(88 %Z)-$\mathbf{P_{h1}}$**) is lower by almost 6000 g·mol^{-1}, compared to **(*Z*)-$\mathbf{P_{h1}}$**. In the case of **(*Z*)-$\mathbf{P_{h2}}$** (resulting from **(*Z*)-$\mathbf{M_{h2}}$**), a smaller apparent M_n value is observed (6000 g·mol^{-1}). The more compact structure of the monomer **(*Z*)-$\mathbf{M_{h2}}$** may lead to a reduction of the hydrodynamic volume of the resulting polymer **(*Z*)-$\mathbf{P_{h2}}$**. Alternatively, the substitution of the alkenyl arm in the ester rotor (shown in green in Figure 1D) may bring the alkene and the acrylate groups residing in the stator in close proximity to each other, facilitating cyclization reactions and thus terminating the polymerization at lower M_n value. Thus, we hypothesize that the combination of these two factors may explain the lower M_n in the second design (**(*Z*)-$\mathbf{P_{h2}}$**). Nevertheless, the M_n values of these polymers are sufficient for performing the targeted photoisomerization studies.

With regard to the optical properties of $\mathbf{P_{h1}}$ and $\mathbf{P_{h2}}$, it is surprising that there is no shift in the UV/Vis absorption spectra of **(*Z*)-$\mathbf{P_{h1}}$** and **(*Z*)-$\mathbf{P_{h2}}$**, and the molar absorptivity of the two polymers are similar (approximately 21000 M^{-1} cm^{-1} at λ_{max} = 372 nm, refer to Figure S2) and in agreement with the literature values for small molecule hydrazone structures.[28] Due to the presence of the (*E*)-isomer (12 %) in **(88 %Z)-$\mathbf{P_{h1}}$**, the absorption spectrum is blue-shifted (Figure S2), as the (*E*)-isomer absorbs photons of higher energy than the (*Z*)-isomer.

With the polymers in hand, we conducted photoisomerization studies of $\mathbf{P_{h1}}$ and $\mathbf{P_{h2}}$ in deuterated toluene (toluene-d_8) monitored by ^{1}H NMR spectroscopy. We selected **(88 %Z)-$\mathbf{P_{h1}}$** and **(*Z*)-$\mathbf{P_{h2}}$** since the two polymers have comparable M_n values (i.e., close to 8000 g·mol^{-1} for **(88 %Z)-$\mathbf{P_{h1}}$** and 6000 g·mol^{-1} for **(*Z*)-$\mathbf{P_{h2}}$**, respectively). We initially adapted the irradiation wavelengths previously employed in the literature.[11b] Accordingly, 410 nm and 365 nm were used for the forward and back photoisomerization, respectively, of the hydrazone core in $\mathbf{P_{h1}}$ and $\mathbf{P_{h2}}$. As can be seen in Figure 2, upon irradiation with blue light (λ = 410 nm, laser power: 6.5 mW ± 12.9 %, up to 3.0·10^{19} photons) the magnetic resonances corresponding to the initial (*Z*)-hydrazone cores in both $\mathbf{P_{h1}}$ and $\mathbf{P_{h2}}$ decrease in intensity, accompanied by the emergence of new resonances associated with the (*E*)-isomer. Aprahamian and colleagues reported an extremely slow thermal back isomerization of the hydrazone cores similar to those in our study, with thermal half-lives up to 3400 years at 25 °C in dimethyl sulfoxide (DMSO).[11b] Indeed, we did not observe any signs of thermal back isomerization (confirmed by ^{1}H NMR spectroscopy, Figure S5–S6) when our irradiated samples were kept in the dark for 4 days at ambient temperature. Therefore, the back isomerization is only possible with light irradiation (at 365 nm in the current study). Accordingly, the polymer solutions previously irradiated with 410 nm blue light were exposed to 365 nm laser-irradiation (laser power: 5.0 mW ± 3.7 %, up to 2.0·10^{19} photons). The ^{1}H NMR spectra of the reaction shown in Figure 2 clearly demonstrate the gradual recovery of the initial (*Z*)-isomer, confirming reversible photoisomerization. In both processes, no additional mag-

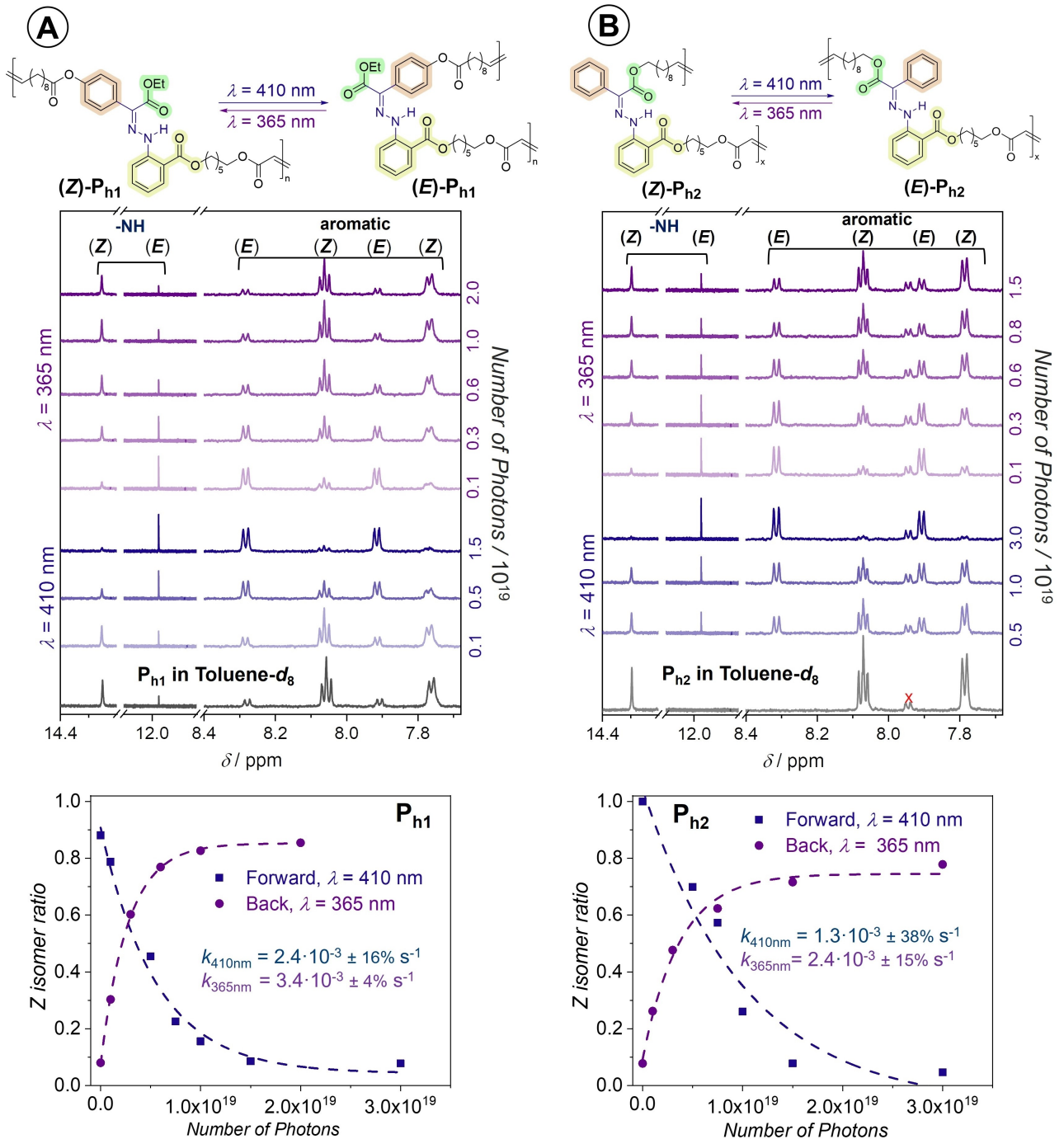

Figure 2. Photoisomerization study of **(88 %Z)-P_{h1}** (A) and **(Z)-P_{h2}** (B): $c_{polymer} = 0.5\ g \cdot L^{-1}$, laser power: 6.5 mW ± 12.9 % at 410 nm, 5.0 mW ± 3.7 % at 365 nm, number of photons (N_p) is calculated from Eq. S1. Top: Stacked ^{1}H NMR spectra recorded in toluene-d_8, 32 scans, at 25 °C. An impurity is noted with a red cross, refer to the main text. Bottom: Kinetic curves fitted with exponential fit functions.

netic resonances aside from those of the isomers were observed in the ^{1}H NMR spectra, suggesting no side reactions and/or degradation of the irradiated polymers.

To quantify and compare the isomerization kinetics of **(88 %Z)-P_{h1}** and **(Z)-P_{h2}** in toluene-d_8 at 25 °C, we plotted the isomerization conversion (determined via an NMR study) *vs* irradiation time.

The number of photons (N_p) is converted to time by rearranging equation S1. The results reveal that polymer **(88 %Z)-P_{h1}** isomerizes faster than polymer **(Z)-P_{h2}** in both the forward and back isomerization (Figure 2, bottom). The associated rate coefficient of the forward isomerization at 410 nm ($k_{f,410nm}$) for **(88 %Z)-P_{h1}** ($2.4 \cdot 10^{-3} s^{-1}$) is almost twice as high as that for **(Z)-P_{h2}** ($1.3 \cdot 10^{-3} s^{-1}$). For the back isomerization at 365 nm, the rate coefficients ($k_{b,365nm}$) are

$3.4 \cdot 10^{-3}\,s^{-1}$ and $2.4 \cdot 10^{-3}\,s^{-1}$ for **(88 %*Z*)-P_{h1}** and **(*Z*)-P_{h2}**, respectively.

Due to the fact that the power of the employed light source (6.5 mW ± 12.9 % for 410 nm irradiation and 5.0 mW ± 3.7 % for the 365 nm irradiation) are much lower than those employed in the literature,[11b,29] a direct comparison of the rate coefficients is challenging. At the photostationary state (PSS) during 410 nm irradiation, both polymers show a high *Z*-to-*E* isomerization conversion (≈92 % (*E*)-isomer for both **(88 %*Z*)-P_{h1}** and **(*Z*)-P_{h2}**). However, for the reversion process at 365 nm irradiation, while the PSS value for the (*Z*)-isomer in **(88 %*Z*)-P_{h1}** is close to the initial ratio (85 % (*Z*)-isomer at PSS 365 nm *vs* 88 % (*Z*)-isomer initially), only around 80 % of the (*Z*)-isomer in **(*Z*)-P_{h2}** is recovered. Data from UV/Vis studies also agree with the NMR spectroscopic results even though we could not quantify the percentage of the (*Z*)- and (*E*)- isomers based on UV/Vis spectra (Figure S3). Changing the solvent from relatively non-polar toluene to aprotic polar dimethylacetamide (DMAc) does not appear to enhance the isomerization of the hydrazone core (Figure S7), suggesting an insignificant contribution of solvent polarity on the photoisomerization efficiency of the studied photoswitch. In the literature, kinetic studies of small molecules similar to the hydrazone core in **(*Z*)-P_{h2}** also reported relatively low conversion for the back isomerization (75 %–86 %).[28–29] In our case, the steric effect inflicted by the *ortho*-substitution of the aliphatic backbone polymer chains connecting the rotor (ester group shown in green in Figure 1D) and the stator (phenyl group shown in yellow in Figure 1D) of the hydrazone core in **(*Z*)-P_{h2}** may compromise the isomerization kinetics as well as the efficiency of the back isomerization. The installation of the photoswitches into the polymer backbone does not reduce their photostability. We demonstrate 6 cycles of photoisomerization without any evidence for photobleaching (Figure S10). It is critical to note that cyclability is in line with the previously reported examples on hydrazone-based polymers.[11,13,23]

We further explore the reliance of the forward isomerization on the absorption wavelength of the hydrazone core, using polymer **(*Z*)-P_{h1}**. Specifically, the number of photons (N_p) was fixed at $2.5 \cdot 10^{18}$ and the molar concentration (0.8 mM) of the chromophore across the irradiation wavelength range (320 nm–430 nm) was kept constant. The results collated in Figure 3 show the highest conversion at close to 390 nm. The shift of the maximum conversion away from the maximum absorption peak of the initial (*Z*)-isomer —although a typical observation for nearly all studied photochemical processes[22]—may partially be due to the spectral overlap between the (*Z*)- and (*E*)-isomers around the peak absorption at 372 nm (Figure 3), interfering with the forward isomerization in the overlapped region. As no difference in the absorption spectra between **(*Z*)-P_{h1}** and **(*Z*)-P_{h2}** is observed, we anticipate a similar action plot for **(*Z*)-P_{h2}**.

Owing to the distinct configuration of the two isomers, (*Z*) and (*E*), we believe the hydrazone photoswitch in the polymer backbone affects the hydrodynamic volume of the polymer during the photoisomerization. The design of $\mathbf{P_{h1}}$ and $\mathbf{P_{h2}}$ suggests that the position of the aliphatic arm in the rotary part of the hydrazone photoswitch in the two polymers (Figure 2, top part) are on opposite sides with respect to the C=N rotation axis. Thus, it appeared to be a viable hypothesis that the two polymers may feature antagonistic changes of their molecular weight distribution upon photo-controlled isomerization.

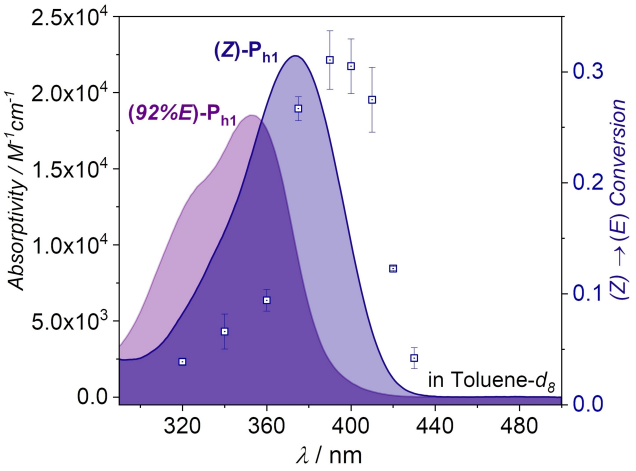

Figure 3. Action plot for the *Z*-to-*E* photoisomerization of **(Z)-P_{h1}** in toluene-d_8 at 25 °C. $c_{hydrazone}$ = 0.8 mM, $N_p = 2.5 \cdot 10^{18}$, laser power: 11.0 mW ± 6.0 %. The absorptivity curve (purple curve) for **(*E*)-P_{h1}** represents the photostationary state (≈92 % (*E*)) during 410 nm irradiation of pristine **(*Z*)-P_{h1}**.

To test the above hypothesis, we recorded and compared Size Exclusion Chromatography (SEC) traces of the non-irradiated and the irradiated polymer solutions (λ = 410 nm, followed by λ = 365 nm in toluene) of $\mathbf{P_{h1}}$ and $\mathbf{P_{h2}}$. Figure 4 demonstrates the antagonistic change of the apparent molecular weight distributions of $\mathbf{P_{h1}}$ and $\mathbf{P_{h2}}$ upon 410 nm laser irradiation. We have shown earlier in the NMR study (Figure 2) that there are no unfavorable reactions, e.g., intra-/intermolecular crosslink, or degradation taking place during the photoisomerization.

Therefore, the shift in the apparent molar mass of $\mathbf{P_{h1}}$ and $\mathbf{P_{h2}}$ upon photoisomerization is attributed to the hydrodynamic volume change of the polymers due to the altered packing density of polymer chains. To quantify these changes, we compared the apparent peak molar mass (M_p) after and before 410 nm irradiation ($\%\Delta M_p = (M_{p,410nm} - M_{p,pristine}) \cdot 100\,\% / M_{p,pristine}$). For polymer $\mathbf{P_{h1}}$, a reduction of approx. 25 % for **(*Z*)-P_{h1}** (with 13 % (*Z*)- and 87 % (*E*)-isomer after 410 nm irradiation) (Figure S4) and close to 22 % for **(88 %*Z*)-P_{h1}** (with 8 % (*Z*)- and 92 % (*E*)-isomer after 410 nm irradiation) (Figure 4, top) was observed. In contrast, polymer **(*Z*)-P_{h2}** displays a 20 % increase in M_p after reaching the photostationary state at 410 nm irradiation (with 8 % (*Z*)- and 92 % (*E*)-isomer) (Figure 4, bottom). Upon back isomerization at 365 nm, the SEC traces of these polymers show a tendency to return to the initial distribution, however not completely (Figure 4 and Figure S4).

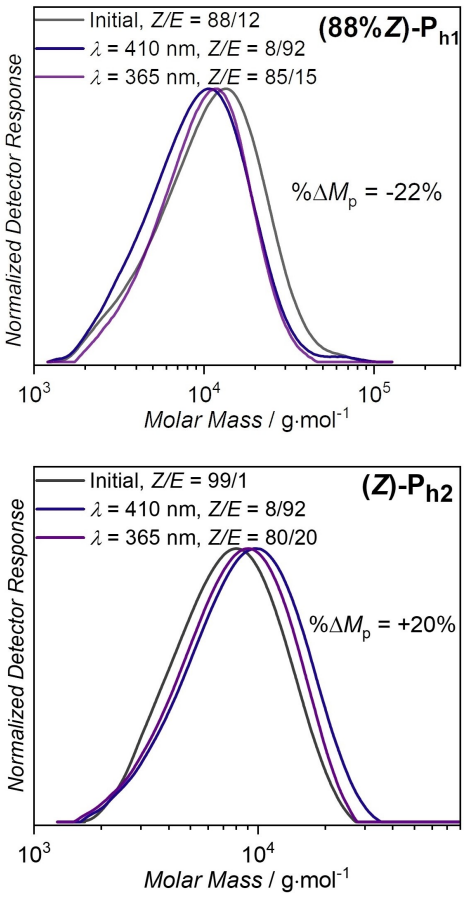

Figure 4. SEC traces recorded in dimethylacetamide (DMAc) during the photoisomerization of $\mathbf{P_{h1}}$ and $\mathbf{P_{h2}}$. Toluene was removed after the photoisomerization reached the target conversion and the residue was redissolved in DMAc. The laser powers were kept in the range of (5.0–6.0) mW. $\%\Delta M_p = (M_{p,410nm} - M_{p,pristine}) \cdot 100\% / M_{p,pristine}$.

Molecular modeling and simulations are indispensable tools for the polymer science community, particularly as those computational approaches enable predictions and provide explanations of experimentally observed macromolecular structures as well as microscopic and macroscopic material properties.[30] Accordingly, four sets of molecular dynamics (MD) simulations were performed. Each set was simulated in triplicate for 500 ns using 10-subunit polymers of the pure *(Z)*- and *(E)*-isomer of both the $\mathbf{P_{h1}}$ and $\mathbf{P_{h2}}$ polymers (in toluene) to characterize the molecular behavior, particularly the impact of the light-induced *Z*-to-*E* isomerization, of each polymer. Initial parameters for each polymer were developed using the Automated Topology Builder (ATB) and manually refined to ensure self-consistency between the polymers and isomerization states (refer to the Supporting Information section 11).

MD simulations revealed distinct conformations between (*Z*)- and *(E)*-isomers for both the $\mathbf{P_{h1}}$ and $\mathbf{P_{h2}}$ polymers. In the simulation, the **(*Z*)-$\mathbf{P_{h1}}$** adopts an extended conformation with an average monomer end-to-end distance of 1.82 ± 0.50 nm. The end-to-end angle—calculated around the imine double bond—was 92 ± 34°. In contrast, **(*E*)-$\mathbf{P_{h1}}$** polymers have a shorter average monomer end-to-end distance of 1.41 ± 0.43 nm (Figure 5, Figure S34 and S35), associated with a more acute angular deflection around the imine double bond of 70 ± 32°, which induces notable kinks throughout the **(*E*)-$\mathbf{P_{h1}}$** polymer. Conversely, each monomer of the **(*Z*)-$\mathbf{P_{h2}}$** polymer contained notable kinks, with an end-to-end angle of 83 ± 34° and an end-to-end distance of 1.50 ± 0.54 nm. These kinks diminished in **(*E*)-$\mathbf{P_{h2}}$**, corresponding to a widening of the end-to-end angle to 115 ± 32° and an associated increase in the monomer end-to-end distance (2.10 ± 0.49 nm), resulting in an extended conformation of the **(*E*)-$\mathbf{P_{h2}}$** polymer (Figure 5, Figure S34 and S35).

The all-atom root mean square deviation (RMSD) calculates the average change in position of each atom of the polymer throughout the simulation, providing a measure of conformational flexibility. A least squares fit was used to progressively fit the ensemble of polymer structures from the 1500 ns of simulations to the initial conformation. The RMSD of the elongated **(*Z*)-$\mathbf{P_{h1}}$** is 1.95 ± 0.38 nm, indicating it has greater conformational flexibility than the kinked and more compact **(*E*)-$\mathbf{P_{h1}}$** which in turn has an RMSD of 1.78 ± 0.29 nm. In contrast, the RMSD of the kinked **(*Z*)-$\mathbf{P_{h2}}$** is 2.08 ± 0.38 nm, displaying less conformational flexibility than the elongated **(*E*)-$\mathbf{P_{h2}}$**, with an RMSD 2.23 ± 0.55 nm (Figure S36). In both $\mathbf{P_{h1}}$ and $\mathbf{P_{h2}}$, the presence of the alkane chains introduces torsional freedom due to the unrestricted rotation of carbon-carbon bonds, enhancing the overall flexibility. Despite this inherent flexibility conferred by the alkane chains, the presence of kinks within the **(*E*)-$\mathbf{P_{h1}}$** and **(*Z*)-$\mathbf{P_{h2}}$** act as localized structural motifs, introducing steric constraints that reduce the conformational flexibility.

The radius of gyration (Figure S37) and effective volume (Figure S38) of each polymer calculated from MD simulations provides a computational measure of the experimental hydrodynamic radius. In $\mathbf{P_{h1}}$, the change of isomerization from **(*Z*)-$\mathbf{P_{h1}}$** to **(*E*)-$\mathbf{P_{h1}}$** corresponds to a reduction in the radius of gyration and effective volume, in agreement with the smaller SEC hydrodynamic radius measured and calculated apparent peak molar mass (M_p) (Figure 4). Consistent with the experimental result, the trend is reversed in $\mathbf{P_{h2}}$ where the change in isomerization from the **(*Z*)-$\mathbf{P_{h2}}$** to **(*E*)-$\mathbf{P_{h2}}$** corresponds to an increase in the radius of gyration, effective volume (Figure S37 and S38), as well as SEC hydrodynamic radius and calculated apparent peak molar mass (M_p) (Figure 4). These results provide a structural rationale for the experimentally observed antagonistic changes in the hydrodynamic radius along the apparent molecular weight distributions of $\mathbf{P_{h1}}$ and $\mathbf{P_{h2}}$ upon irradiation (Figure 4).

These data demonstrate that by altering the substitution site of the main-chain arm, the behavior of a key macromolecular property, i.e., the hydrodynamic volume, can be manipulated. We submit that the properties of these materials in the solid-state, e.g., their glass transition temperature (T_g), are also affected by photoisomerization. It is well known that the T_g of a polymer can be critically influenced by *cis* and *trans* configurations in the polymer as the volume, chain stiffness and interchain cohesion of

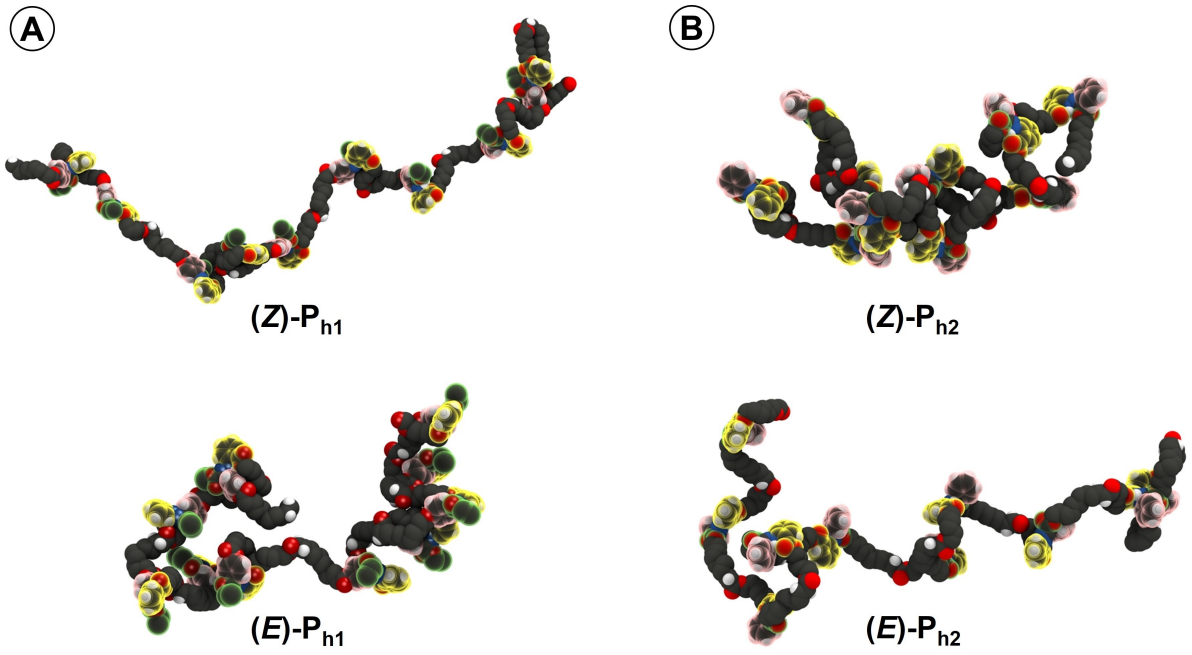

Figure 5. Representative conformation of the $\mathbf{P_{h1}}$ (A) and $\mathbf{P_{h2}}$ (B) polymers from replicate MD simulations. The snapshot taken from the first simulation of the three 500 ns replicate simulations gives the conformation of **(Z)-P$_{h1}$**, **(*E*)-P$_{h1}$**, **(*Z*)-P$_{h2}$**, and **(*E*)-P$_{h2}$** after 466.6 ns, 447.2 ns, 461.3 ns, and 455.4 ns of MD simulation, respectively. The phenyl stator is highlighted in yellow. The phenyl ring decoration of the rotor is highlighted in pink. The ester moiety in the rotor is highlighted in green.

polymer chains are greatly affected via *cis* and *trans* configurations.[27,31] In fact, Aprahamian and colleagues have illustrated a photomodulation of T_g on a series of polyacrylate- and polymethacrylate-based polymers bearing hydrazone-based side chains.[23] In the current study, we investigate the role of photoisomerization on the resulting T_g of the reported main-chain polymers ($\mathbf{P_{h1}}$ and $\mathbf{P_{h2}}$), employing Differential Scanning Calorimetry (DSC).

We initially examined the thermal stability of the studied polymers (**(88 %*Z*)-P$_{h1}$** and **(*Z*)-P$_{h2}$**) using ThermoGravimetric Analysis (TGA). The temperature at which 5 % mass is lost, $T_{d,5\%}$, is 298 °C for **(88 %*Z*)-P$_{h1}$** and 302 °C **(*Z*)-P$_{h2}$** (Figure S9), indicating the two polymers have excellent thermal stability despite their relatively low apparent average molar masses (M_n = (6000–8000) g·mol^{-1}). These values, i.e., $T_{d,5\%}$, are similar to those reported for main-chain α-bisimine ADMET polymers.[18] We subsequently conducted DSC measurements of the pristine and irradiated polymers. The sample preparation conditions (i.e., solvent, temperature) were kept identical (refer to Supporting Information for the detailed protocol). Solutions of **(88 %*Z*)-P$_{h1}$** and **(*Z*)-P$_{h2}$** in dichloromethane (DCM) (1.0 g·L^{-1}) were irradiated with 400 nm LEDs (10 W) for 4 h (> 93 % *Z*-to-*E* conversion). It is important to note that the pristine samples were prepared in a similar manner. As the solvent residues—originating from the preparation of the DSC sample material—can also behave as unwanted plasticizers, the pristine and irradiated samples (concentrated to 100 g·L^{-1} in DCM, which has considerably lower boiling point compared to toluene and DMAc) were drop-cast in separate DSC pans and dried at 25 °C in vacuum for 3 days prior to DSC measurement. The DSC thermograms depicted in Figure 6 show a T_g of 6.2 °C and 0.5 °C for the pristine **(88 %*Z*)-P$_{h1}$** and **(*Z*)-P$_{h2}$**, respectively. The higher M_n and an additional ester group in **(88 %*Z*)-P$_{h1}$** may explain the higher glass transition temperature (T_g) determined for **(88 %*Z*)-P$_{h1}$**. Aprahamian and colleagues ob-

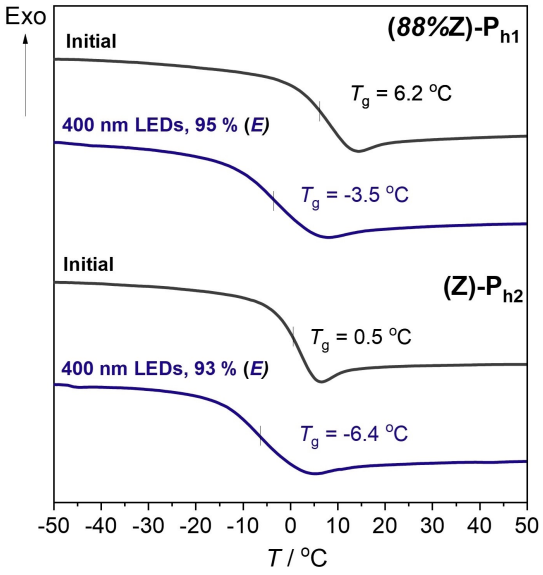

Figure 6. Stacked DSC thermograms of **(88 %*Z*)-P$_{h1}$**, **(*Z*)-P$_{h2}$** and the corresponding irradiated polymers. Conditions: 2 cycles of heating and cooling from −100 °C to 90 °C at 20 °C·min^{-1} in a nitrogen atmosphere. The depicted DSC curves are taken from the second heating cycle.

served a decrease in T_g of side-chain hydrazone polymers with the longer aliphatic chain connected to the ester rotary part (highlighted in green in Figure 1D).[23] Thus, a low T_g (0.5 °C) is not unexpected for **(88 %*Z*)-P_{h1}**. Upon forward isomerization (>93 % (*E*)-isomer at the photostationary state (PSS) at 400 nm (λ_{max}) irradiation), both irradiated polymers show a decrease in T_g, i.e., a difference in T_g value (ΔT_g) before and after forward isomerization, of 9.7 °C for the irradiated **(88 %*Z*)-P_{h1}** and a ΔT_g of 6.9 °C for the irradiated **(*Z*)-P_{h2}** (Figure 6). The observed ΔT_g is in contrast to the results reported earlier for the side-chain approach.[23] In other words, when hydrazones are introduced as pendant groups, only one part (rotor or stator) of the photoswitch is connected to the polymer chain, leaving the other part unhindered. Consequently, this facilitates a tighter packing of the chromophores, i.e., hydrazones, which are of an aromatic nature upon forward isomerization (i.e., *Z*/*E*), leading to higher T_g.[23] In our case, however, both stator and rotor of the photoswitch are tethered to the polymer backbone through aliphatic carbon chains (C6–C11). As a result, the hydrazone photoswitches are surrounded by soft segments (i.e., aliphatic chains). In the case of **P_{h1}**, the structural change upon blue light irradiation enables these soft segments to closely pack. Further, there is no melting/crystallization process observed in the DSC thermograms (Figure 6). Thus, the packing of such soft aliphatic chains driven by photoisomerization is the likely reason for the lower T_g (−3.5 °C) of the irradiated **P_{h1}**.

In contrast, **(*Z*)-P_{h2}** resembles a polystyrene-type polymer with the phenyl rotary as the pendant group (the orange group shown in Figure 1D, 2B). These groups can be considered as a part of the hard segment. Upon *Z*-to-*E* photoisomerization, the aggregation of these aromatic phenyl groups may be disturbed due to the polymer volume expansion, coupled with geometry of the resulting (*E*)-isomer disfavoring their tight packing. Consequently, these factors can be accountable for the negative T_g (−6.4 °C) of **P_{h2}** measured after forward isomerization.

Interestingly, the close inspection of the (*E*)-configuration of **P_{h1}** in Figure 2A, i.e., **(*E*)-P_{h1}**, indicates that the geometry may allow for the aggregation of the ethyl ester groups (the rotor highlighted in green). The structure of **P_{h1}** mimics an acrylate-type polymer, i.e., a polyester. It has been shown that non-conjugated polymers, e.g., polyesters, are capable of fluorescence (even when they are not conjugated) possibly due to the cluster formation and non-covalent interactions among the functional groups, e.g., ester groups.[32] This phenomenon, known as aggregation-induced emission (AIE), is induced by the alignment of polymer chains, which in turn undergo changes during the isomerization, thereby affecting the fluorescence behavior. In order to validate the latter assumption, we recorded fluorescence spectra of the pristine and irradiated polymers (Figure S8) and note that only the **(*E*)-P_{h1}** polymers (95 % (*E*), resulting from **(88 %*Z*)-P_{h1}** via irradiation) emitted light at λ_{max} ≈650 nm under 425 nm excitation (Figure S8). Additionally, the aggregation of these ethyl ester groups may additionally contribute to the drop in T_g of **P_{h1}** observed in the DSC study.

Conclusion

We introduce the synthesis of main-chain hydrazone-based polymers (**P_{h1}** and **P_{h2}**) via head-to-tail ADMET polymerization, followed by a detailed photoisomerization study, including a photochemical action plot. Importantly, we demonstrate that the hydrazone core with two ester groups substituted in *ortho*-position act as strong H-acceptors to prevent the coordination of the Ru-based HG-II catalyst with the hydrazone functional group, allowing ADMET polymerization featuring hydrazone as the main-chain photoswitch. By switching the substitution locations of the arm in the rotor of the hydrazone photoswitch, we demonstrate an antagonistic change in the hydrodynamic volume (between 20 % and 25 % changes in M_p) of the resulting polymers (**P_{h1}** and **P_{h2}**) upon forward photoisomerization, which was explored also via molecular modeling and simulations. The simulations thus allowed us to understand that an adoption of a kinked monomer conformation in **(*E*)-P_{h1}** and **(*Z*)-P_{h2}** induces a more condensed polymer structure, corresponding to a more acute end-to-end angle and shorter end-to-end distance, resulting in smaller effective volumes when compared to the more flexible and less ordered **(*Z*)-P_{h1}** and **(*E*)-P_{h2}**. Critically, the photoisomerization behavior strongly affects the macroscopic physical properties of the polymers, particularly the T_g, which features negative values, thus implying a plasticizing effect. As both the (*Z*)- and (*E*)-isomers of the polymers revealed T_g values lower than ambient temperature, photoinduced solid-to-liquid transition was not possible. However, the photoswitchable T_g behavior is convincing to suggest that a judicious molecular design would allow developing main-chain-type hydrazone decorated polymers that show visible or near-infrared light-induced solid-to-liquid transitions. Our study thus opens possibilities to manipulate the properties of photoresponsive polymeric materials in a predetermined and flexible fashion.

Supporting Information

The authors have cited additional references within the Supporting Information.[33] Simulation parameter files, and the initial and final coordinates of the simulations are available at https://github.com/OMaraLab/Hydrazone_Photoswitches.

Acknowledgements

C. B.-K. acknowledges the Australian Research Council (ARC) for funding in the context of a Laureate Fellowship enabling his photochemical research program. The authors acknowledge funding for the project from QUT's Centre for Materials Science. The Central Analytical Research Facility (CARF) at QUT is gratefully acknowledged. H. M. acknowledges the University of Haute-Alsace (UHA) for the financial support from the French National Research Agency (ANR) with the reference "ANR-22-CPJ1-0077-01"

and from the CNRS for a junior professorship contract. H. M. and J. F. acknowledge financial support from the Karlsruhe Institute of Technology, in addition to the Federal Ministry of Education and Research (BMBF) and the Baden-Württemberg Ministry of Science as part of the Excellence Strategy of the German Federal and State Governments. C. B.-K. acknowledge additional funding by the Deutsche Forschungsgemeinschaft (DFG, German Research Foundation) under Germany's Excellence Strategy for the Excellence Cluster '3D Matter Made to Order' (EXC-2082/1—390761711). M. L. O. acknowledges the computational resources from the National Computational Infrastructure (NCI Australia), an NCRIS enabled capability supported by the Australian Government. We thank Prof. I. Aprahamian (Dartmouth College) and his colleagues along Dr. T. R. Guimarães (QUT, University of Bordeaux) for valuable discussions, particularly on the synthesis of the hydrazone monomer in design **1**. We acknowledge Prof. K. Thurecht, Dr. C. Bell and F. McCallum (Centre for Advanced Imaging, The Queensland University) for access to the DSC characterization.

Conflict of Interest

The authors declare no conflict of interest.

Data Availability Statement

The data that support the findings of this study are available from the corresponding author upon reasonable request.

Keywords: ADMET Polymerization · Hydrazone · Main-Chain Polymers · Photoswitch

[1] a) S. Chatani, C. J. Kloxin, C. N. Bowman, *Polym. Chem.* **2014**, *5*, 2187–2201; b) J. Hobich, E. Blasco, M. Wegener, H. Mutlu, C. Barner-Kowollik, *Macromol. Chem. Phys.* **2023**, *224*, 2200318.

[2] a) S. Liang, S. Li, C. Yuan, D. Zhang, J. Chen, S. Wu, *Macromolecules* **2023**, *56*, 448–456; b) P. H. Nguyen, A. M. Scheuermann, A. Nikolaev, M. L. Chabinyc, C. M. Bates, J. Read de Alaniz, *ACS Appl. Polym. Mater.* **2023**, *5*, 4698–4703; c) F. Zhao, L. Grubert, S. Hecht, D. Bléger, *Chem. Commun.* **2017**, *53*, 3323–3326.

[3] a) D. Beery, E. Stanisauskis, G. M. McLeod, A. Das, G. A. Guillory, J. G. Kennemur, W. S. Oates, K. Hanson, *ACS Appl. Polym. Mater.* **2022**, *4*, 4081–4086; b) D. Villarón, S. J. Wezenberg, *Angew. Chem.* **2020**, *132*, 13292–13302.

[4] a) K. Imato, K. Momota, N. Kaneda, I. Imae, Y. Ooyama, *Chem. Mater.* **2022**, *34*, 8289–8296; b) C. Li, A. Iscen, L. C. Palmer, G. C. Schatz, S. I. Stupp, *J. Am. Chem. Soc.* **2020**, *142*, 8447–8453.

[5] a) H. M. Tran, T. H. Nguyen, V. Q. Nguyen, P. H. Tran, L. D. Thai, T. T. Truong, L.-T. T. Nguyen, H. T. Nguyen, *Macromol. Res.* **2019**, *27*, 25–32; b) S. Rahimi, S. Stumpf, O. Grimm, F. H. Schacher, U. S. Schubert, S. Schubert, *Biomacromolecules* **2020**, *21*, 3620–3630.

[6] a) J. Jiang, Q. Chen, M. Xu, J. Chen, S. Wu, *Macromol. Rapid Commun.* **2023**, *44*, 2300117; b) H. Nie, N. S. Schauser, J. L. Self, T. Tabassum, S. Oh, Z. Geng, S. D. Jones, M. S. Zayas, V. G. Reynolds, M. L. Chabinyc, *J. Am. Chem. Soc.* **2021**, *143*, 1562–1569.

[7] F. Xu, B. L. Feringa, *Adv. Mater.* **2023**, *35*, 2204413.

[8] A. Abdollahi, B. Ghasemi, S. Nikzaban, N. Sardari, S. Jorjeisi, A. Dashti, *ACS Appl. Mater. Interfaces* **2023**, *15*, 7466–7484.

[9] P. Weis, D. Wang, S. Wu, *Macromolecules* **2016**, *49*, 6368–6373.

[10] a) L. Greb, A. Eichhöfer, J. M. Lehn, *Eur. J. Org. Chem.* **2016**, *2016*, 1243–1246; b) L. Greb, H. Mutlu, C. Barner-Kowollik, J.-M. Lehn, *J. Am. Chem. Soc.* **2016**, *138*, 1142–1145; c) L. D. Thai, T. R. Guimaraes, S. Spann, A. S. Goldmann, D. Golberg, H. Mutlu, C. Barner-Kowollik, *Polym. Chem.* **2022**, *13*, 5625–5635.

[11] a) H. Qian, S. Pramanik, I. Aprahamian, *J. Am. Chem. Soc.* **2017**, *139*, 9140–9143; b) A. Ryabchun, Q. Li, F. Lancia, I. Aprahamian, N. Katsonis, *J. Am. Chem. Soc.* **2019**, *141*, 1196–1200.

[12] B. Shao, I. Aprahamian, *Molecular Photoswitches: Chemistry, Properties, and Applications*, Wiley-VCH, Weinheim, **2022**, pp. 113–129.

[13] D. J. van Dijken, P. Kovaříček, S. P. Ihrig, S. Hecht, *J. Am. Chem. Soc.* **2015**, *137*, 14982–14991.

[14] H. Yu, T. Iyoda, T. Ikeda, *J. Am. Chem. Soc.* **2006**, *128*, 11010–11011.

[15] C. Gäbert, D. Hicke, J. Bahnemann, L. Mayerhofer, M. Hartlieb, S. Reinicke, *Macromol. Rapid Commun.* **2023**, *44*, 2300108.

[16] T. Kawai, Y. Nakashima, M. Irie, *Adv. Mater.* **2005**, *17*, 309–314.

[17] G. R. Gossweiler, T. B. Kouznetsova, S. L. Craig, *J. Am. Chem. Soc.* **2015**, *137*, 6148–6151.

[18] L. D. Thai, T. R. Guimaraes, L. C. Chambers, J. A. Kammerer, D. Golberg, H. Mutlu, C. Barner-Kowollik, *J. Am. Chem. Soc.* **2023**, *145*, 14748–14755.

[19] S. M. Landge, E. Tkatchouk, D. Benítez, D. A. Lanfranchi, M. Elhabiri, W. A. Goddard III, I. Aprahamian, *J. Am. Chem. Soc.* **2011**, *133*, 9812–9823.

[20] L. Ding, J. Li, T. Li, L. Zhang, W. Song, *React. Funct. Polym.* **2017**, *121*, 15–22.

[21] Y. Lin, M. H. Barbee, C.-C. Chang, S. L. Craig, *J. Am. Chem. Soc.* **2018**, *140*, 15969–15975.

[22] I. M. Irshadeen, S. L. Walden, M. Wegener, V. X. Truong, H. Frisch, J. P. Blinco, C. Barner-Kowollik, *J. Am. Chem. Soc.* **2021**, *143*, 21113–21126.

[23] S. Yang, J. D. Harris, A. Lambai, L. L. Jeliazkov, G. Mohanty, H. Zeng, A. Priimagi, I. Aprahamian, *J. Am. Chem. Soc.* **2021**, *143*, 16348–16353.

[24] M. D. Schulz, K. B. Wagener, *ACS Macro Lett.* **2012**, *1*, 449–451.

[25] H. Abd El-Wahab, *Prog. Org. Coat.* **2015**, *89*, 106–113.

[26] R. R. Kumar, R. Ramesh, J. G. Małecki, *J. Organomet. Chem.* **2018**, *862*, 95–104.

[27] C. Appiah, G. Woltersdorf, R. A. Pérez-Camargo, A. J. Müller, W. H. Binder, *Eur. Polym. J.* **2017**, *97*, 299–307.

[28] Q. Li, H. Qian, B. Shao, R. P. Hughes, I. Aprahamian, *J. Am. Chem. Soc.* **2018**, *140*, 11829–11835.

[29] Q. Qiu, S. Yang, M. A. Gerkman, H. Fu, I. Aprahamian, G. G. Han, *J. Am. Chem. Soc.* **2022**, *144*, 12627–12631.

[30] T. E. Gartner III, A. Jayaraman, *Macromolecules* **2019**, *52*, 755–786.

[31] J. Brandrup, E. H. Immergut, E. A. Grulke, *Polymer Handbook*, Wiley, New York, **1999**

[32] K. Bauri, B. Saha, A. Banerjee, P. De, *Polym. Chem.* **2020**, *11*, 7293–7315.

[33] a) A. K. Malde, L. Zuo, M. Breeze, M. Stroet, D. Poger, P. C. Nair, C. Oostenbrink, A. E. Mark, *J. Chem. Theory Comput.* **2011**, *7*, 4026–4037; b) L. Wang, K. Zhu, W. Cao, C. Sun, C.

Lu, H. Xu, *Polym. Chem.* **2019**, *10*, 2039–2046; c) N. Schmid, A. P. Eichenberger, A. Choutko, S. Riniker, M. Winger, A. E. Mark, W. F. Van Gunsteren, *Eur. Biophys. J.* **2011**, *40*, 843–856; d) E. F. Pettersen, T. D. Goddard, C. C. Huang, G. S. Couch, D. M. Greenblatt, E. C. Meng, T. E. Ferrin, *J. Comput. Chem.* **2004**, *25*, 1605–1612; e) M. J. Abraham, T. Murtola, R. Schulz, S. Páll, J. C. Smith, B. Hess, E. Lindahl, *SoftwareX* **2015**, *1*, 19–25; f) G. Bussi, D. Donadio, M. Parrinello, *J. Chem. Phys.* **2007**, *126*, 014101; g) H. J. Berendsen, J. v. Postma, W. F. Van Gunsteren, A. DiNola, J. R. Haak, *J. Chem. Phys.* **1984**, *81*, 3684–3690; h) M. L. Waskom, *J. Open Source Software* **2021**, *6*, 3021; i) J. D. Hunter, *Comput. Sci. Eng.* **2007**, *9*, 90–95; j) W. Humphrey, A. Dalke, K. Schulten, *J. Mol. Graphics* **1996**, *14*, 33–38; k) J. P. Menzel, B. B. Noble, A. Lauer, M. L. Coote, J. P. Blinco, C. Barner-Kowollik, *J. Am. Chem. Soc.* **2017**, *139*, 15812–15820.

Manuscript received: October 20, 2023
Accepted manuscript online: November 21, 2023
Version of record online: December 20, 2023